Wax Inhibition by Comb-like Polymers: Support of the Incorporation−Perturbation Mechanism from Molecular Dynamics Simulations

Yun Hee Jang,[†,§] Mario Blanco,[†] Jefferson Creek,[‡,⊥] Yongchun Tang,[‡,⊥] and William A. Goddard, III*[,†]

Materials and Process Simulation Center (MC139-74), California Institute of Technology, Pasadena, California 91125, and Chevron Energy Technology Company, 1600 Smith Street, Houston, Texas 77002

Received: April 10, 2007; In Final Form: July 26, 2007

Deposition of wax on a cold surface is a serious problem in oil production. Progress in developing more effective wax inhibitors has been impeded by the lack of an established mechanism connecting the molecular structure to inhibitor efficiency. Some comb-like polymers having long alkyl side chains are known to decrease the rate of wax formation. Among several possible mechanisms, we investigate here the *incorporation−perturbation* mechanism. According to this mechanism, the inhibitor molecules in oil are preferentially partitioned (*incorporation*) toward the wax-rich (amorphous) wax deposits (soft wax), which then serves as a *perturbation* to slow down the ordering transition of soft amorphous wax into more stable but problematic hard wax crystals. Indeed, molecular dynamics simulations on an effective inhibitor molecule in both the oil phase and in the amorphous wax phase support the idea that the oil-to-wax partition of the inhibitor is energetically favorable. With the inhibitor molecule embedded, the structure of wax crystal is disturbed, significantly decreasing the order and significantly lowering the cohesive energy density relative to that of the pure wax crystal, supporting the slower transition from soft wax to hard wax. Thus, in the presence of an effective wax inhibitor, crystallization (formation of hard wax) is slowed dramatically, so that there is time to flush out the soft wax with a high-pressure flow inside the pipeline. This suggests design principles for developing improved wax inhibitors.

1. Introduction

One of the serious problems in oil production, particularly in the deep-water production, is the deposition of wax on the oil pipe walls.[1−7] This occurs when high-melting-point components in the hot crude oil, usually high-molecular-weight alkanes called paraffins, contact cold pipe walls (Scheme 1).[8−10] The rate of wax deposit is controlled by the wax content in the crude oil and by the temperature gradient between the outside cold temperature and that inside the pipeline. The wax deposit causes flow problems in oil production and transportation.

Several polymers having long alkyl side chains, so-called "comb-like" polymers, are known to decrease the rate of wax formation (Scheme 1).[7,11−17] Acrylate and methacrylate polymers have been known for several decades as commercial flow improvers and wax inhibitors,[8,11,18,19] but none is sufficiently effective. Other more complex backbones containing nitrogen have shown some improvement. Progress in developing more effective inhibitors has been impeded by the lack of an established mechanism connecting the molecular structure to inhibitor efficiency. In this study we used molecular dynamics (MD) techniques to investigate the enthalpic aspect of the molecular-level interaction between a wax and a wax inhibitor in oil. This interaction is believed to be sufficient to explain the observed wax inhibition process at a few parts per million.

SCHEME 1: Wax Formation (Upper) and Its Inhibition by Comb-like Polymers (Lower)

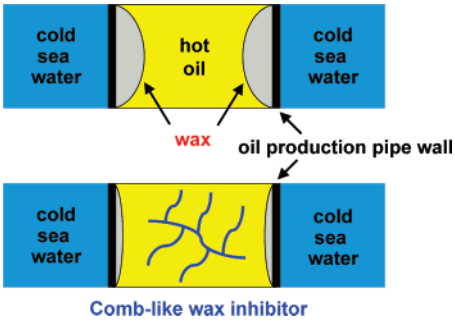

Speculations on the steps of wax formation lead to several possible mechanisms of wax inhibition, each of which might block or at least slow down one of the steps.

Mechanism 1 (Sequestering). Above the wax melting temperature, paraffin molecules are still soluble in oil. However, when the temperature cools down below a certain point, high-molecular-weight paraffin can form a solid phase (wax). This temperature is called the wax appearance temperature (WAT). Certain chemicals (wax inhibitors) can lower the WAT and slow down the wax formation process. One of the possible mechanisms of these inhibitors is that they might bind to paraffin molecules quite favorably out of the oil phase because of the favorable van der Waals (vdW) interaction of the long paraffin chains with the long side chains of the inhibitors. It is our hypothesis that the association constant between inhibitor and

* To whom correspondence should be sent. Phone: 626-395-2731. Fax: 626-585-0918. E-mail: wag@wag.caltech.edu.
† California Institute of Technology.
‡ Chevron Energy Technology Company.
§ Present Address: Department of Materials Science and Technology, Gwangju Institute of Science and Technology (GIST), Gwangju 500-712, Korea; LEMA, Université François Rabelais, Tours 37200, France.
⊥ Present Address: Power, Environmental & Energy Research (PEER) Center, California Institute of Technology, Covina, CA 91722.

10.1021/jp072792q CCC: $37.00
Published on Web 11/02/2007

wax molecule might play a role in lowering the WAT. These favorable interactions would significantly lower the chance that the paraffin molecules gather together to form wax aggregates, thereby slowing down or blocking the nucleation process.

Mechanism 2 (Incorporation−Perturbation). When the solution temperature nears the cloud temperature (or WAT), wax molecules start to gather together to form wax aggregates. These wax aggregates incorporate wax inhibitors when present. Once the inhibitor molecules have been incorporated into the wax aggregates, their presence perturbs or retards the ordering transformation of the amorphous wax aggregate (soft wax) into the problematic ordered phase (hard wax). This delay favors the chance that the wax aggregates are swept away in the oil production streamflow before the wax hardens.

Mechanism 3 (Inhibitor Adsorption on Wax Crystals). In this mechanism, inhibitors are preferentially adsorbed on the wax nuclei growing surfaces. Their presence blocks the growth of hard wax deposits. The overall effect of surface blocking is to reduce the WAT and to slow down the wax deposition process. This has been investigated in a modeling study of Duffy and co-workers.[20−22]

Mechanism 4 (Inhibitor Adsorption on Pipe Walls). It is also possible that inhibitors are adsorbed on pipe walls favorably. Adsorption of inhibitors on pipe walls would provide an irregular surface, thereby inhibiting the adsorption and diffusion of paraffin molecules to form wax crystals on cold pipe walls.

Among the various hypotheses of the wax inhibition mechanism, we consider that the formation of soft wax (Mechanism 2) is the most likely the process. In our internal laboratory tests, a gel-like wax is formed in the early deposition stage. However, it is not clear whether the formation of the gel-like (amorphous) wax is favored thermodynamically. Thus, our study focuses on investigating the behavior of wax inhibitor molecules in an oil phase on an amorphous wax phase and in a crystalline wax phase, processes which underscore the incorporation−perturbation mechanism (Mechanism 2).

Our hypothesis is as follows: if an inhibitor tends to co-aggregate with wax molecules (i.e., preferentially incorporate into a wax aggregate from the oil phase), the presence of the inhibitor inside the wax aggregate would retard the ordering transformation (second step of wax formation) of the amorphous wax aggregate (soft wax) into the problematic ordered phase (hard wax), because the cohesive energy density (CED) of the crystalline wax, which is essentially the driving force of the ordering transformation, would be much smaller in the presence of an entangled inhibitor inside. Thus, formation of the hard wax would be delayed in the presence of the inhibitors, allowing the soft wax aggregate to exist long enough that it could be wiped out by the streamflow before forming the hard wax. A key test of this hypothetical mechanism is to determine whether inhibitors tend to be incorporated preferentially into the wax aggregates out of the oil phase. We investigated this mechanism by MD calculations of the energetics of the following steps.

A. Incorporation of a Comb-like Wax Inhibitor from the Oil Phase into the Still Amorphous Wax Phase Is Energetically Favorable. This is shown in Section 4 by calculating the *incorporation energy* (E_{incorp}), the energy change between the two states, before and after incorporation (Scheme 2). Because the actual incorporation process is difficult to simulate, and since the initial- and final-state energetics are pathway independent (thermodynamic state functions), we instead approximated the *before-incorporation energy* (E_{before}) as the sum of the energies of two separate systems:

SCHEME 2: Incorporation Energy of an Inhibitor from Oil to Wax

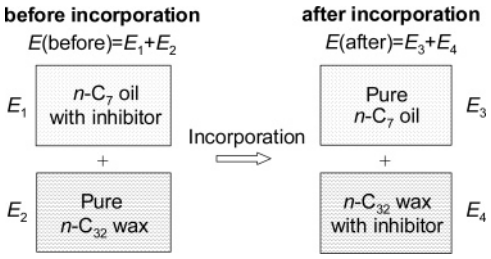

SCHEME 3: Incorporation−Perturbation Mechanism of Wax Inhibition[a]

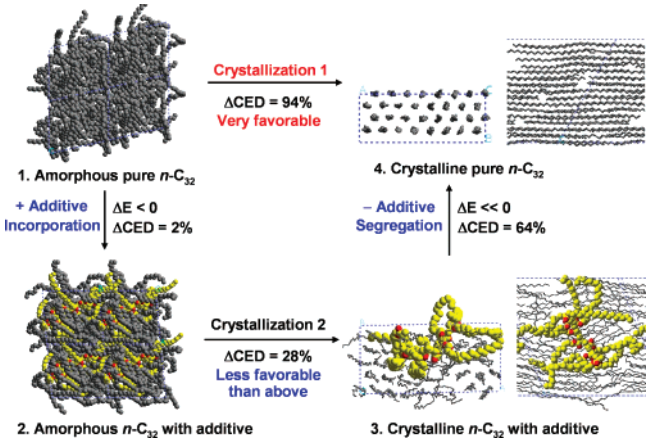

[a] Once inhibitors (shown in yellow and red) are incorporated favorably from oil into amorphous wax (both shown in gray) (1 → 2), the crystallization of the soft wax into the hard wax is perturbed and delayed by the presence of the inhibitor inside (2 → 3 rather than 1 → 4). The delayed crystallization is eventually completed with the favorable release of the inhibitors back into the oil phase (3 → 4). Overall, the hard wax is formed by the route of 1 → 2 → 3 → 4. This process is expected to be much slower than a direct crystallization 1 → 4. Thus, in the presence of inhibitor, the hard wax formation would be delayed, allowing the soft wax more time to be wiped out by the streamflow.

(1) oil with an inhibitor inside (upper left; E_1), and

(2) pure wax (amorphous or crystalline) (lower left; E_2).

Likewise, the *after-incorporation energy* (E_{after}) was approximated as the sum of the energies of two separate systems:

(3) pure oil (upper right; E_3);

(4) wax with an inhibitor inside (lower right; E_4).

Then, E_{incorp} is given by

$$E_{incorp} = E_{after} - E_{before} = (E_3 + E_4) - (E_1 + E_2) \quad (1)$$

B. The Ordering Transition from Amorphous to Crystalline Wax is Less Favorable in the Presence of the Perturbation from Comb-like Wax Inhibitors Inside. This is shown in Section 5 by calculating the *CED*s of four related systems (Scheme 3):

(1) pure amorphous wax (upper left),

(2) amorphous wax containing an inhibitor inside (lower left),

(3) pure crystalline wax (upper right), and

(4) crystalline wax containing an inhibitor inside (lower right).

We use an oligomer of poly(octadecyl acrylate) (PODA), one of the most promising wax inhibitors, as the model inhibitor. The amorphous wax phase was modeled by a periodic bath of liquid-like *n*-dotriacontane (*n*-C_{32}), and the crystalline wax phase

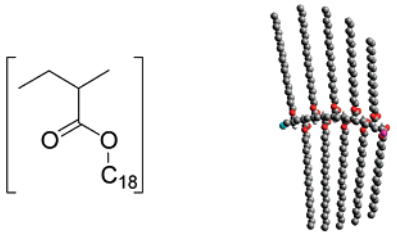

(a) PODA (b) PAA1

Figure 1. Wax inhibitor PODA and its model PAA1.

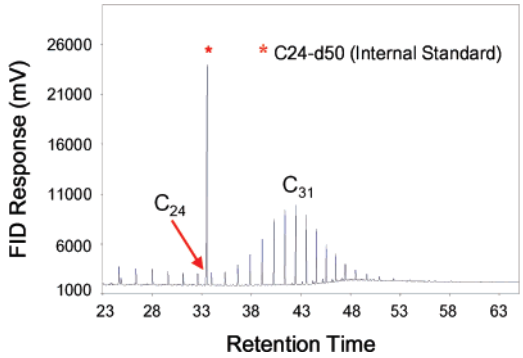

Figure 2. Deposit from a Gulf of Mexico crude oil. Temperature = 16 °C, cooling water temperature = 5 °C, flow velocity = 37 m/min (2 ft/s), and deposition time = 60 min (ref 23).

was modeled by a periodic cell of well-ordered *n*-C_{32}. The oil phase was modeled by a periodic bath of liquid-phase *n*-heptane (*n*-C_7).

2. Calculation Details

2.1. Model Inhibitor. A comb-like wax inhibitor is characterized by its backbone structure, tail length (number of carbons in a long alkyl tail), and spacer width (number of short tails between adjacent long tails). Different spacer widths are represented by the different number ratios between long tails and short tails. The performance, which is represented by the inverse of the amount of wax deposited in the presence of the inhibitor, varies across these structures.

Acrylate polymers with long alkyl side chains have been known as effective commercial flow improvers.[8,12] PODA is one of the most representative comb-like wax inhibitors (Figure 1 and Table 1). A decamer of syndiotactic PODA (PAA1, MW 3276) was chosen as a model inhibitor representing the PODA. A degree of polymerization of 10 might be too small to model a polymeric moiety, but a PODA with 8−10 monomer units was shown to inhibit wax formation,[11] as was a poly(octadecyl methacrylate) with a degree of polymerization of 10−11.[23]

2.2. Model Oil, Model Wax. We chose *n*-C_7 (T_m = 182.586 K;[24] T_b = 371.6 K[25,26]) as the oil solvent and *n*-C_{32} (T_m = 342.5 K;[26,27] T_b = 740.2 K[26,28]) as the wax compound of theoretical modeling. A mixture of paraffin wax compounds between C_{24} to C_{36} with a peak at C_{31} were used in the laboratory testing (Figure 2). The *n*-C_{32} is one of the components having the largest contributions. The *n*-C_{32} was the largest fraction in another testing.[6]

2.3. Force Field (FF) for *n*-Alkanes (Oil, Wax, Tail of Inhibitor). The methylene (CH_2) and methyl (CH_3) groups in *n*-alkanes (oil solvent, wax, and long alkyl tails of inhibitors) were treated as united atoms, that is, each CH_2 or CH_3 unit was treated as a single neutral pseudoatom. The FF for these united atoms was mostly taken from the Siepmann−Karanorni−Smit (SKS) FF.[29−31] The bond-stretching force constant, which is not in the original SKS FF, was taken from the AMBER FF.[32,33] The torsion potential of the SKS FF had been taken from the optimized potentials for liquid simulation (OPLS) FF.[34] The FF is described in detail in the Supporting Information (Table S1). The nonbonded interactions between 1 and 2, 1 and 3, and 1 and 4 neighbors were excluded, and other nonbonded interactions were truncated by a cubic spline cutoff function defined as 1 for $r < 13.8$ Å, 0 for $r > 14.3$ Å, and decreasing smoothly in between. The off-diagonal vdW parameters between CH_2 and CH_3 are given by the geometric means of the diagonal terms:

$$R_0^{AB} = \sqrt{R_0^A R_0^B} \text{ and } D_0^{AB} = \sqrt{D_0^A D_0^B}$$

2.4. FF for the Backbone of the Inhibitor. The FF for the acrylate backbone was mostly taken from the OPLS FF developed for liquid methyl acetate[35,36] except for the modifications described below. Again, the FF is described in detail in the Supporting Information (Table S2 and Figures S1 and S2).

Atomic charges of the acrylate backbone (−CHCOO−) were refined by ab initio quantum mechanics (QM) calculation (HF/6-31G**; *Jaguar*, version 3.5)[37,38] on a model compound representing the acrylate group, $(CH_3)_2CHCOOCH_2CH_3$ (Figure S1a,b). The resulting atomic charges were reasonably similar to those used in the OPLS FF (Figure S1c).

The force constants for bond stretching, angle bending, and inversion, which are not in the original OPLS FF, were taken from the AMBER FF (Figure S2b,c).[32,33]

The torsion FF was refined to reproduce the QM torsion potential curves (HF/6-31G**) on small model compounds such as $(CH_3CH_2)_2CHCOOCH_3$, $(CH_3)_2CHCOOCH_2CH_3$, and CH_3-$COOCH_2CH_2CH_3$ (Figures S3 and S4). The details are described in the Supporting Information (Section S2).

3. Simulation Results: Each Piece

3.1. Oil Bath (Pure Oil). The oil bath was modeled by a periodic cell of liquid-phase *n*-C_7 [*n*-$C_7(l)$] at 293 K (Figure 3a). The simulation temperature was set to 293 K (20 °C), consistent with the wax-forming temperature in wax deposit experiments on a cold finger. The experimental runs typically are done under the following conditions: the oil temperature is 18−35 °C, the cold finger temperature is 10−18.5 °C, and the wax deposit starts to block pipes at 15−17 °C.[23]

The initial unit cell was built as a cubic box of 37.75 Å on each side, which contains 221 *n*-C_7 molecules at its experimental density at 293 K, 0.6838 g/cm^3.[26,39] This size of the unit cell is large enough to immerse a fully extended conformation of model inhibitor and/or model wax molecule without any extrusion out of the cell. The initial torsion angles of 221 *n*-C_7 molecules at 293 K were assigned randomly on the basis of the three-state rotational isomeric states (RIS) model of *n*-alkanes: 0.0 kcal/

TABLE 1: Characteristics and Performance (Inverse of the Amount of Wax Deposit g/day) of PODA Wax Inhibitor and Its Model PAA1

	backbone	tail	C_{18}/C_1	MW	wax deposit
inhibitor PODA model PAA1	alkyl acrylate	C_{18}	1:0	19 000 (59 C_{18}) 3276 (10 C_{18})	13.69 g/day (blank: 72)

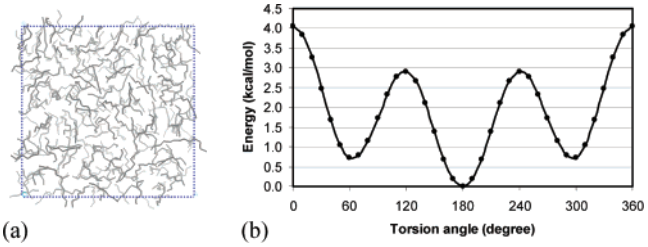

Figure 3. (a) Unit cell of the model oil bath of 221 n-C_7 molecules. (b) Torsion PE around the central bond of n-hexane calculated with the current FF, which leads to the three-state RIS model of n-alkanes (0.0 kcal/mol for t; 0.72 kcal/mol for g^+ and g^-).

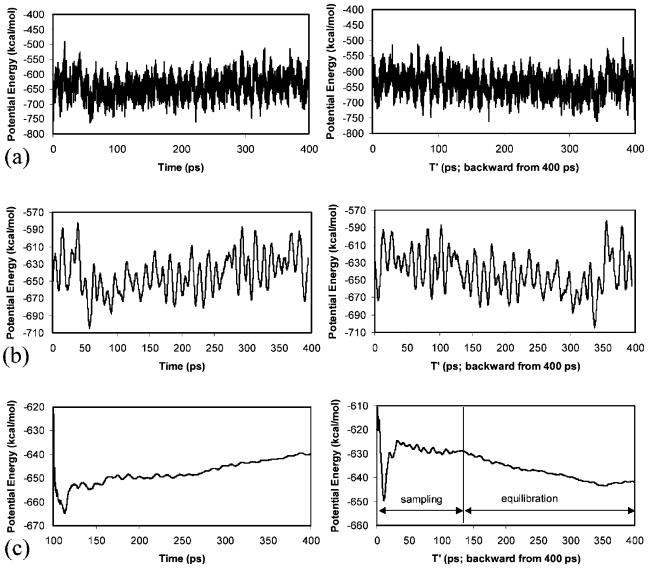

Figure 4. PE profiles of a bath of 221 n-C_7 molecules during the NPT MD simulation: (a) PE; (b) 5-ps block averages of PE; (c) running averages of PE taken from 100 ps to each time. Profiles taken and averaged backward from the end of the simulation (400 ps) are shown on the right panel. The PE profile averaged backward (right panel of c) shows that it took about 270 ps to equilibrate the bath.

TABLE 2: Properties of the Model Oil Bath (221 n-C_7 Molecules)

	calculation	experiment
density (ρ; g/cm^3)	0.672 (293 K)	0.6838 (293 K) 0.6795 (298 K)[a]
ΔH_{vap} (kcal/mol)	8.9 ± 0.3 (293 K)	8.74 ± 0.01 (298 K) 8.52 (313 K)[b]
solubility parameter (δ; MPa$^{1/2}$)	15.2 (293 K)	15.1 (298 K)[a]

[a] References 26 and 39. [b] References 25 and 41−43.

mol at 180° (trans; t) and 0.72 kcal/mol at 60° and 300° (gauche; g^+ and g^-) (Figure 3b).[34]

The bath was then subjected to the NVT MD simulations for 100 ps and then NPT simulation for 400 ps in a time step of 1 fs. All the simulations were carried out using *Cerius2* software.[40]

The potential energy (PE) profile along the simulation time (Figure 4), especially the backward average profile shown in Figure 4c, shows that the oil bath was equilibrated by 270 ps. Thus, properties such as density, molar heat of vaporization (ΔH_{vap}), and solubility parameter (Table 2) were calculated by taking averages over the final 125 ps of the NPT simulation after the 275-ps equilibration period. The error of each property was estimated from the standard deviation between four block averages taken every 25 ps.

The calculated density was 0.672 g/cm^3, in agreement with the experimental values of 0.6838 g/cm^3 (293 K) and 0.6795 g/cm^3 (298 K).[26,39] The PE averaged to −2.89 ± 0.02 kcal/mol per chain [$E(l)$]. In combination with the average PE of a single chain of n-C_7 in the gas phase ($E(g)$; 5.4 ± 0.3 kcal/mol from 150-ps MD after 50-ps equilibration), this leads to ΔH_{vap}[n-C_7-(l)] of 8.9 ±0.3 kcal/mol from the relation

$$\Delta H_{vap} = E(g) - E(l) + P\Delta V \approx E(g) - E(l) + PV_m(g) = E(g) - E(l) + RT \qquad (2)$$

where $P\Delta V \approx PV_m(g) = RT = 0.58$ kcal/mol at 293 K. This is in agreement with the experimental value of 8.74 ± 0.01 kcal/mol (298 K).[25,41−43] The solubility parameter (or Hildebrand parameter) is defined as[26,39]

$$\delta = c^{0.5} = \left(-\frac{U_m}{V_m}\right)^{0.5} = \left(\frac{\Delta H_{vap} - RT}{V_m}\right)^{0.5} \qquad (3)$$

where c is the CED, $-U_m$ is the molar internal energy (the molar PE of a material relative to the ideal vapor at the same temperature (that is, $\Delta H_{vap} - RT$), and V_m is the molar volume. The average V_m of 248.0 Å^3 was obtained by dividing the average cell volume by 221, the number of chains in a unit cell. This resulted in a solubility parameter of 15.2 MPa$^{1/2}$, in agreement with the experimental value of 15.1 MPa$^{1/2}$ (298 K).[26,39]

In order to check the reproducibility of the simulation, two separate oil baths were built from the same three-state RIS ratio as used above. The unit cell size for those baths was set to 37.96 Å on each side on the basis of the volume obtained from the NPT simulation. These baths were then independently subjected to NVT simulation for 600 ps, and the averages were taken during the last 300 ps after a 300-ps equilibration period. The error was estimated from the standard deviation between three block averages taken every 100 ps. The resulting average pressures were satisfactorily low (−0.0004 ± 0.0011 and −0.0007 ± 0.0019 GPa). The average PEs from both simulations were essentially the same (−2.89 ± 0.01 and −2.90 ± 0.02 kcal/mol/chain, which we averaged to −2.89 ± 0.02 kcal/mol/chain or −639 ± 5 kcal/mol/cell), showing good reproducibility.

3.2. Initial Wax Aggregate (Pure Soft Wax). We assumed an initial soft wax aggregate to be a bath of long n-alkane chains with a liquid-like, random packing (which we call "amorphous wax" below). This amorphous wax phase was modeled with a periodic bath of liquid-phase n-C_{32} [n-C_{32}(l)].

The initial unit cell was built as a cubic box of 26.42 Å on each side, which contained 20 n-C_{32} chains at the experimental liquid-phase density of n-C_{32} at 293 K, 0.8124 g/cm^3.[26] The initial torsion angles at 293 K were randomly chosen according to the same three-state RIS ratio. Again, to ensure reproducibility, three unit cells were built separately and submitted to independent runs: a minimization first and then to an NVT MD simulation at 293 K for 400 ps. The properties were averaged over the final 300 ps after the 100-ps equilibration, and the standard deviations were taken between the final three 100-ps block averages. The average PEs of these three runs are close enough to each other: −67 ± 3, −64 ± 2, and −62.1 ± 0.6 kcal/mol. The second cell with a mid-value of ⟨PE⟩ (−64 ± 2 kcal/mol) was chosen and subjected further to an NPT MD simulation for 400 ps. The average properties were estimated in the same way.

TABLE 3: Properties of Amorphous and Crystalline Model Waxes (n-C_{32}) with or without PAA1 Inhibitor Inside

	calcd$^{293\ K}$	exptl
	(a) n-C_{32} (amorphous)	
density (ρ; g/cm^3)	0.816 ± 0.003	0.8124$^{293\ K}$
ΔH_{vap} (kcal/mol)	32.0 ± 0.8	35.1 ± 0.2$^{456\ K}$
CED (MPa)	237 ± 6 (100%)[a]	
	(b) n-C_{32} (crystalline)	
density (ρ; g/cm^3)	0.9556 ± 0.0002	0.9604$^{293\ K}$
ΔH_{vap} (kcal/mol)	52.8 ± 0.8	53.44 ± 0.24$^{298\ K}$
CED (MPa)	464 ± 7 (195%)[a]	
	(c) PAA1/n-C_{32} (amorphous)	
CED (MPa)	244 ± 3 (103%)[a]	
	(d) PAA1/n-C_{32} (crystalline)	
CED (MPa)	311 ± 2 (131%)[a]	

[a] In parentheses are given the relative CED values with respect to that of the amorphous n-$C_{32}(l)$ phase. The increase from c to d is not as big as the increase from a to b.

The final snapshot after the NPT simulation is shown in Scheme 3 (upper left). The average density was estimated as 0.816 ± 0.003 g/cm^3, in agreement with the experimental value (0.8124 g/cm^3).[26] The average PE was estimated as −64 ± 5 kcal/mol/unit cell or −3.2 ± 0.2 kcal/mol/chain [$E(l)$]. In combination with the average PE of a single chain of n-C_{32} in the gas phase [n-$C_{32}(g)$] of over 150 ps after 50 ps equilibration [$E(g)$; 28.2 ± 0.8 kcal/mol], this leads to 32.0 ± 0.8 kcal/mol as ΔH_{vap}[n-$C_{32}(l)$] (eq 2). We could not find an experimental value for ΔH_{vap}[n-$C_{32}(l)$] reported at (or converted to) 298 K, but ΔH_{vap}[n-$C_{32}(l)$] at 456 K is reported as 35.1 ± 0.2 kcal/mol.[44] Combining with the average volume of each chain (V_m; 918 ± 4 Å^3) (eq 3), this leads to CED[n-$C_{32}(l)$] of 237 ± 6 MPa [= (342 ± 9) × 10^{-4} kcal/mol/Å^3] with respect to the n-$C_{32}(g)$ as the reference state (Table 3a).

The trans-to-gauche (t/g) ratio of torsion angles was calculated as 67:33, which lies within the normal range of liquid or liquid-like n-alkanes.[45,46]

3.3. Crystalline Wax (Pure Hard Wax). We assumed the problematic hard wax to be a crystalline wax after an ordering transformation of the amorphous wax aggregate. The crystalline wax was modeled with a periodic cell of ordered n-C_{32} chains.

The initial unit cell was built from the 8 × 2 × 1 supercell of the monoclinic crystal structure of n-C_{32} [n-$C_{32}(cr)$; a = 5.57 Å, b = 7.42 Å, c = 43.26 Å, β = 119.3°; space group $P2_1/a$; two chains per cell; density ρ = 0.9604 g/cm^3].[47] It had 32 n-C_{32} chains in each unit cell. It was subjected to minimization, then to a 100-ps NVT MD simulation, and then finally to a 200-ps NPT MD simulation at 293 K. Properties were averaged for 150 ps after a 50-ps equilibration period, and the error of each property was estimated as the standard deviation between the final three 50-ps block averages.

The final snapshot of the NPT simulation is shown in Scheme 3 (upper right). The average density was estimated as 0.9556 ± 0.0002 g/cm^3, again in agreement with the experimental value at 293 K (0.9604 g/cm^3).[47] The average PE was estimated as −770 ± 2 kcal/mol/cell or −24.06 ± 0.06 kcal/mol/chain [$E(cr)$]. Combined with an $E(g)$ of 28.2 ± 0.8 kcal/mol, this leads to 52.8 ± 0.8 kcal/mol of the molar heat of sublimation (ΔH_{sub}) of n-$C_{32}(cr)$ at 293 K:

$$\Delta H_{sub} = E(g) - E(cr) + RT\ (= PV = 0.58\ \text{kcal/mol}) \qquad (4)$$

This is in agreement with the experimental value at 298 K, 53.44 kcal/mol.[44] Combining with V_m of n-$C_{32}(cr)$ (783.5 ± 0.2 Å^3) (eq 3), this leads to 464 ± 7 MPa [= (668 ± 10) × 10^{-4} kcal/mol/Å^3] as the CED of n-$C_{32}(cr)$ at 293 K with respect to n-$C_{32}(g)$ as the reference state (Table 3b).

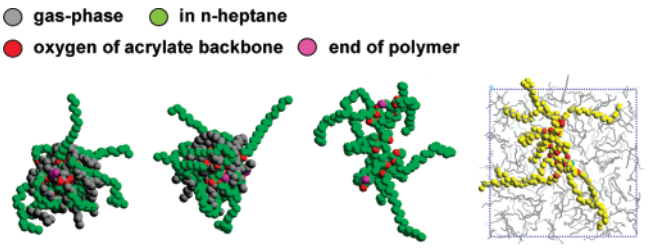

Figure 5. PAA1 viewed in three different directions. Superimposed are its gas-phase structure (gray; average surface area = 2116 ± 78 Å^2) and its solution-phase structure (green; average surface area = 3464 ± 72 Å^2) taken out of the n-C_7 oil bath shown in the right panel.

SCHEME 4: Scheme To Insert a Big Solute Molecule (Wax Inhibitor or Wax Molecule Itself) in a Solvent Box, Avoiding Too Much Initial Overlap between the Solute and Solvent Molecules

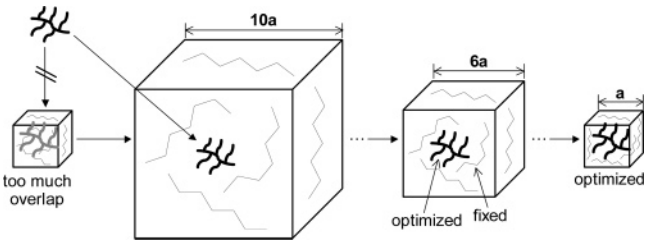

The increase of the CED from the amorphous value was estimated to be as large as 95.5% (Table 3a to 3b).

3.4. Oil Bath with an Inhibitor. An initial syndiotactic PAA1 homopolymer was built in the ideal all-trans conformation, and then the initial torsion angles were randomly assigned at 293 K according to the RIS table determined from the FF described in Section 2. Two separate initial structures were built, and each was submitted to the MD simulation in the gas phase for 800 ps. Both gas-phase simulations ended up with the inhibitor in a very compact and globular structure, consistent with a maximum in the intramolecular contacts (Figure 5, gray). Over 400 ps after a 400-ps equilibration, the Connolly surface area of PAA1 was averaged to 2116 ± 78 Å^2, and the PE was averaged to 202 ± 4 kcal/mol.

Then, the final gas-phase structures were independently immersed into the n-C_7 oil bath using the insertion scheme shown in Scheme 4,[48] which helps to avoid the overlap between solute (PAA1) and solvent molecules (221 n-C_7 molecules).

Step 1. The n-C_7 bath is first expanded into a cell 10 times larger in each cell parameter to yield enough space to accommodate the solute without overlap.

Step 2. PAA1 is then inserted at the center of the cell.

Step 3. The cell is scaled down gradually (in four steps) toward the target volume, giving the right density [~0.6838 g/cm^3 of n-$C_7(l)$].[26,39] At each step, the solute is minimized and equilibrated with fixed solvent molecules around it.

Step 4. At the final target volume, the whole cell is minimized and equilibrated.

Step 5. It is subjected to an NPT simulation or to an NVT simulation after adjusting the volume so that it gives an average pressure of zero.

The final structures were submitted to the annealing dynamics simulation up to 793 K and then NVT dynamics at 293 K for 460 ps. The backward average profile of PE (Figure 6) shows the bath has been well equilibrated through this procedure. The

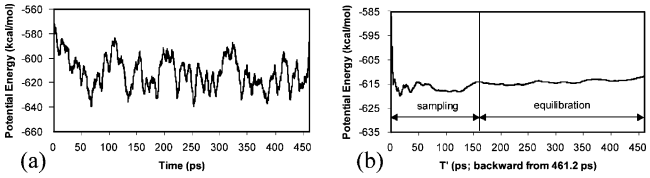

Figure 6. PE profiles of a bath containing PAA1 inhibitor and 221 *n*-C_7 molecules during the NPT MD simulation: (a) 5-ps block averages of PE and (b) averages taken backward from 460 ps, which shows the bath was well equilibrated.

average PEs of the two separate runs are -603.2 ± 0.7 and -612 ± 11 kcal/mol, which are averaged to -608 ± 12 kcal/mol.

The representative snapshot (Figure 5, green) shows that the inhibitor tends to extend its conformation (open up) in the *n*-C_7 bath. The Connolly surface area of PAA1 is 3464 ± 72 A^2 in the *n*-C_7 bath (averaged over 160 ps after a 300-ps equilibration), and this is larger by 64% than its gas-phase value. This is the result of replacing vdW interaction between hydrocarbon chains by favorable interactions with neighboring solvent molecules without folding the inhibitor itself. The backbone attained a helical conformation, and the side chains were arranged in a spiral fashion. Intramolecular interactions between long alkyl chains were not particularly observed.

3.5. Amorphous Wax with an Inhibitor. PAA1 was taken out of the final structure in an *n*-C_7 oil bath and immersed into the final structure of a pure soft wax phase using the same insertion scheme described in Section 3.4. The composite phase was subjected to a minimization, a 100-ps NVT MD, and then a 400-ps NPT MD simulation at 293 K.

The final snapshot is shown in Scheme 3 (lower left). The amorphous wax with PAA1 in it does not look very different from the pure amorphous wax. The PE was averaged to -82 ± 9 kcal/mol. Combining this with the average PEs of gas-phase PAA1 and *n*-C_{32} (202 ± 4 and 28.2 ± 0.8 kcal/mol, respectively), the enthalpy of vaporization of the composite cell is estimated as 860 ± 10 kcal/mol from the definition

$$\Delta H_{\mathrm{vap}}^{\mathrm{comp}} = E(g;\ \mathrm{PAA1}) + 20\,E(g;\ n\text{-}C_{32}) - E(l;\ \mathrm{PAA1\ in\ 20}\ n\text{-}C_{32}) + 21\,RT \quad (5)$$

Combining this result with the average volume of the unit cell (24156 ± 73 Å^3), this leads to a CED of 244 ± 3 MPa [$= (351 \pm 4) \times 10^{-4}$ kcal/mol/Å^3] (eq 3). The CED of this composite system is not very different (3% increase) from the CED of the pure amorphous wax (Table 3, a to c), indicating essentially no disruption by the inhibitor at the initial soft stage of the wax aggregate.

3.6. Crystalline Wax with an Inhibitor. PAA1 was also immersed into the final structure of pure crystalline wax phase. The composite phase was subjected to a minimization, a 100-ps NVT MD, and then a 400-ps NPT MD simulation at 293 K.

The final snapshot is shown in Scheme 3 (lower right). Contrary to an inhibitor in the amorphous wax, an inhibitor inside the crystalline wax perturbed the ordered crystal structure a great deal. From the PE averaged to -395 ± 7 kcal/mol, the enthalpy of sublimation for the composite cell is estimated as 1519 ± 9 kcal/mol from the definition

$$\Delta H_{\mathrm{sub}}^{\mathrm{comp}} = E(g;\ \mathrm{PAA1}) + 32\,E(g;\ n\text{-}C_{32}) - E(cr;\ \mathrm{PAA1\ in\ 32}\ n\text{-}C_{32}) + 33\,RT \quad (6)$$

Combining this result with the average volume of the unit cell (33314 ± 34 Å^3), the CED was estimated as 311 ± 2 MPa [$= (450 \pm 3) \times 10^{-4}$ kcal/mol/Å^3]. This value is much smaller (by 33.0%) than the CED of the pure crystalline wax (Table 3, b to d), indicating a great deal of disruption by the inhibitor in the later stage of hard wax formation.

TABLE 4: Incorporation Energy of an Inhibitor from Oil to Wax

average PE (kcal/mol)	(a) into Soft wax	(b) into Hard wax
	before incorporation	
n-C_7 with PAA1: E_1	-608 ± 11	-608 ± 11
pure *n*-C_{32}: E_2	-64 ± 5 (*l*)	-770 ± 2 (*cr*)
E_{before} ($= E_1 + E_2$)	-672 ± 12	-1378 ± 11
	after incorporation	
pure *n*-C_7: E_3	-639 ± 5	-639 ± 5
n-C_{32} with PAA1: E_4	-82 ± 9 (*l*)	-395 ± 7 (*cr*)
E_{after} ($= E_3 + E_4$)	-721 ± 10	-1034 ± 9
	incorporation energy	
E_{incorp} ($= E_{\mathrm{after}} - E_{\mathrm{before}}$)	-49 ± 16	344 ± 14

4. Discussion: Incorporation−Perturbation

4.1. Incorporation of the Inhibitor. Collecting the average PEs of all relevant systems based on Scheme 2 and eq 1 [Table 4(a)] gives -49 ± 16 kcal/mol as the incorporation energy when an inhibitor (PAA1) is transferred from oil [*n*-C_7(*l*)] into amorphous wax [*n*-C_{32}(*l*)]. Thus, at least from the enthalpic point of view, the inhibitor should be favorably incorporated from the oil phase into the wax phase in the early-stage (amorphous, liquid-like, soft wax) aggregates, getting ready to perturb it later on.

4.2. Perturbation by the Inhibitor. The driving force of the crystallization of wax is closely related to the amount of the CED gain during the transformation from the amorphous phase to the crystalline phase. As summarized in Scheme 3 and Table 3, whereas the CED of pure wax (pure *n*-C_{32}) is 95% higher in the crystalline phase than in the amorphous phase (Table 3, a to b), the CED of wax in the presence of an inhibitor (PAA1) inside is only 28% higher in the crystalline phase than that in the amorphous phase (Table 3, c to d). This is the result of a partially ordered crystalline phase in the presence of the inhibitor. This result implies that, once an inhibitor is incorporated into the amorphous (soft) wax phase, the crystallization of this soft wax into the more problematic hard wax, having lost a big portion of the driving thermodynamic enthalpy, could be delayed significantly.

4.3. Release of Inhibitor from Hard Wax. Contrary to the incorporation into an amorphous wax, the incorporation of an inhibitor (PAA1) from oil [*n*-C_7(*l*)] into crystalline wax [*n*-C_{32}(*cr*)] requires a huge amount of energy (344 ± 14 kcal/mol; Table 4b), obviously because the presence of the inhibitor disrupts the energetics of the high ordering of the pure crystalline wax. The inhibitor appears to be more stable in the oil phase rather than in the crystalline wax phase, and thus it should be eventually released out of the wax crystal. Thus, although the crystallization of wax could be delayed by the presence of inhibitors, the inhibitors will be released back into the oil phase, leaving the crystalline wax behind in the long run.

On the basis of these results, we suggest that the role of the comb-like wax inhibitors could be only to delay the crystallization of wax, increasing the chance that the soft wax can be wiped out in the meantime by the streamflow in the pipes. The inhibitor is unable to completely stop the crystallization process.

Recently we conducted some experimental work to confirm this hypothesis. In general, the inhibition efficiency decreases with time.

5. Summary

We used MD simulation techniques to investigate the molecular-level behavior of a wax inhibitor (modeled by PAA1, a model of PODA) in oil (modeled by 221 *n*-C_7 chains) and in wax (modeled by 20−32 *n*-C_{32} chains) at a wax-forming temperature in search for plausible molecular-level mechanisms of wax inhibition. We found that the comb-like inhibitor in oil and in amorphous wax prefers an open, extended, spiral conformation rather than a compact one, which would have the most favorable interaction with the oil solvent. Consequently, the incorporation of this inhibitor from the oil phase into an amorphous *soft* wax phase is expected to be favorable, leading to a negative (exothermic) incorporation energy. However, this bulging conformation of the inhibitor makes it a significant perturbation inside a well-ordered crystalline wax phase, leading to a much lower CED than that for a pure wax crystal. This leads to the incorporation−perturbation mechanism of wax inhibition, in which the presence of an inhibitor favorably incorporated into an amorphous soft wax phase dramatically reduces the tendency for the ordering transformation of the soft wax into a crystalline *hard* wax, delaying the transformation.

This suggests that, in designing effective wax inhibitors, one should use a comb-like structure in which the side arms are of such a length as to interact favorably with the fraction of the oil most likely to crystallize into the hard wax phase. Our experimental studies suggest that, for a typical oil in which the molecular weight of the dominant components corresponds to ∼C_{26}−C_{32}, the composition of the hard wax components tend to correspond to ∼C_{50}−C_{62}. In this case, our simulations suggest that the optimum side chain on the comb-like inhibitor should correspond to ∼C_{28} (28 = 56/2) with a spacing along the backbone of approximately three carbons. It might be good to have some variation in the side chain lengths, say 25 to 31 in the above case.

Acknowledgment. This research was supported by Chevron Energy Technology Company and by the NSF (CMMI-0727870). Some of the calculations were carried out at NCSA (U. Illinois). The facilities of the MSC used in this work are supported by grants from DOE-ASCI, ARO/DURIP, ARO/MURI, NIH, NSF, Chevron-Texaco, Intel Components Research, Dow-Corning, Nissan, Pfizer, Boehringer-Ingelheim, and Sanofi-Aventis.

Supporting Information Available: Description of the FF for *n*-alkanes (oil, wax, and tail of inhibitor) and for the backbone of the inhibitor. This material is available free of charge via the Internet at http://pubs.acs.org.

References and Notes

(1) Misra, S.; Baruah, S.; Singh, K. *SPE Prod. Facil.* **1995**, *10*, 50−54.
(2) Brown, T. S.; Niesen, V. G.; Erickson, D. D. *JPT, J. Pet. Technol.* **1995**, *47*, 328−329.
(3) Li, M. Y.; Su, J. G.; Wu, Z. L.; Yang, Y. D.; Ji, S. L. *Colloids Surf. A: Physicochem. Eng. Aspects* **1997**, *123*, 635−649.
(4) El-Emam, N. A.; Bayoumi, A. W. A.; El-Gamal, I. M.; Abu-Zied, A. *Oil Gas J.* **1993**, 70−79.
(5) Addison, G. E. *SPE J.* **1984**, *13391*, 203−210.
(6) Machado, A. L. C.; Lucas, E. F. *J. Appl. Polym. Sci.* **2002**, *85*, 1337−1348.
(7) Alvares, D. R. S.; Menezes, S. M. C.; Lucas, E. F. *Polym. Int.* **2004**, *53*, 1639−1643.
(8) El-Gamal, I. M.; Ghuiba, F. M.; El-Batanoney, M. H.; Gobiel, S. *J. Appl. Polym. Sci.* **1994**, *52*, 9−19.
(9) Le, H. T. U.S. Patent 4886520, 1989.
(10) Claudy, P.; Letoffe, J.-M.; Bonardi, B.; Vassilakis, D.; Damin, B. *Fuel* **1993**, *72*, 821−827.
(11) Kern, R.; Dassonville, R. *J. Cryst. Growth* **1992**, *116*, 191−203.
(12) Talroze, R. V.; Zubarev, E. R.; Rogunova, M. A.; Litvinov, I. A.; Plate, N. A.; Udipi, K.; Kruse, R. *Polym. Adv. Technol.* **1996**, *7*, 182−186.
(13) Kim, H.; Jung, J. C.; Zin, W.-C. *Polymer* **1996**, *37*, 2573−2576.
(14) Alvares, D. R. S.; Lucas, E. F. *Pet. Sci. Technol.* **2000**, *18*, 195−202.
(15) Groffe, D.; Groffe, P.; Takhar, S.; Andersen, S. I.; Stenby, E. H.; Lindeloff, N.; Lundgren, M. *Pet. Sci. Technol.* **2001**, *19*, 205−217.
(16) Wang, K. S.; Wu, C. H.; Creek, J. L.; Shuler, P. J.; Tang, Y. C. *Pet. Sci. Technol.* **2003**, *21*, 359−368.
(17) da Silva, C. X.; Alvares, D. R. S.; Lucas, E. F. *Energy Fuels* **2004**, *18*, 599−604.
(18) Chatterjee, A. K.; Phatak, S. D.; Murthy, P. S.; Joshi, G. C. *J. Appl. Polym. Sci.* **1994**, *52*, 887−894.
(19) Sifferman, T. R. *J. Pet. Technol.* **1979**, *31*, 1042−1050.
(20) Duffy, D. M.; Rodger, P. M. *J. Phys. Chem. B* **2002**, *106*, 11210−11217.
(21) Duffy, D. M.; Rodger, P. M. *Phys. Chem. Chem. Phys.* **2002**, *4*, 328−334.
(22) Duffy, D. M.; Moon, C.; Rodger, P. M. *Mol. Phys.* **2004**, *102*, 203−210.
(23) Colussi, A. J.; Hoffmann, M. R.; Tang, Y. *Langmuir* **2000**, *16*, 2405−2408.
(24) Holzhauer, J. K.; Ziegler, W. T. *J. Phys. Chem.* **1975**, *79*, 590−604.
(25) Majer, V.; Svoboda, V.; Kehiaian, H. V. *Enthalpies of Vaporization of Organic Compounds. A Critical Review and Data Compilation*; International Union of Pure Applied Chemistry; Blackwell Scientific Publications: Oxford, 1985.
(26) *CRC Handbook of Chemistry and Physics*, 80th ed.; CRC Press: Boca Raton, FL, 1999−2000.
(27) Pouillot, F. L. L.; Chandler, K.; Eckert, C. A. *Ind. Eng. Chem. Res.* **1996**, *35*, 2408−2413.
(28) *CRC Handbook of Data on Organic Compounds*, 2nd ed.; CRC Press, Inc.: Boca Raton, FL, 1989.
(29) Siepmann, J. I.; Karaborni, S.; Smit, B. *Nature* **1993**, *365*, 330−332.
(30) Smit, B.; Karaborni, S.; Siepmann, J. I. *J. Chem. Phys.* **1995**, *102*, 2126−2140.
(31) Martin, M. G.; Siepmann, J. I. *J. Am. Chem. Soc.* **1997**, *119*, 8921−8924.
(32) Weiner, S. J.; Kollman, P. A.; Case, D. A.; Singh, U. C.; Ghio, C.; Alagona, G.; Profeta, S.; Weiner, P. *J. Am. Chem. Soc.* **1984**, *106*, 765−784.
(33) Weiner, S. J.; Kollman, P. A.; Nguyen, D. T.; Case, D. A. *J. Comput. Chem.* **1986**, *7*, 230−252.
(34) Jorgensen, W. L.; Madura, J. D.; Swenson, C. J. *J. Am. Chem. Soc.* **1984**, *106*, 6638−6646.
(35) Briggs, J. M.; Nguyen, T. B.; Jorgensen, W. L. *J. Phys. Chem.* **1991**, *95*, 3315−3322.
(36) Jorgensen, W. L.; Briggs, J. M.; Contreras, M. L. *J. Phys. Chem.* **1990**, *94*, 1683−1686.
(37) *Jaguar*, v3.5; Schrodinger, Inc.: Portland, OR, 1998.
(38) Greeley, B. H.; Russo, T. V.; Mainz, D. T.; Friesner, R. A.; Langlois, J.-M.; Goddard, W. A., III; Donnelly, Jr., R. E.; Ringnalda, M. N. *J. Chem. Phys.* **1994**, *101*, 4028−4041.
(39) Brandrup, J.; Immergut, E. H. *Polymer Handbook*, 3rd ed.; John Wiley & Sons: New York, 1989.
(40) *Cerius2*, v3.5; Molecular Simulations, Inc.: San Diego, CA, 1997.
(41) Ruzicka, K.; Majer, V. *J. Phys. Chem. Ref. Data* **1994**, *23*, 1−39.
(42) Chickos, J. S.; Wilson, J. A. *J. Chem. Eng. Data* **1997**, *42*, 190−197.
(43) Cox, J. D.; Pilcher, G. *Thermochemistry of Organic and Organometallic Compounds*; Academic Press: London and New York, 1970.
(44) Piacente, V.; Fontana, D.; Scardala, P. *J. Chem. Eng. Data* **1994**, *39*, 231−237.
(45) Clavell-Grunbaum, D.; Strauss, H. L.; Snyder, R. G. *J. Phys. Chem. B* **1997**, *101*, 335−343.
(46) Wunderlich, B.; Moller, M.; Grebowicz, J.; Baur, H. In *Conformational Motion and Disorder in Low and High Molecular Mass Crystals*; Springer-Verlag: Berlin, 1988; p 48.
(47) Nyburg, S. C.; Potworowski, J. A. *Acta Cryst.* **1973**, *B29*, 347−352.
(48) Belmares, M. P. Ph.D. Thesis, Division of Chemistry, California Institute of Technology, Pasadena, 1998.